# Phonon spectroscopy of lithium-doped KBr

Werner Zoller
*Technical University of Munich, Munich, West Germany*

Frank Bridges
*Technical University of Munich, Munich, West Germany*
*and University of California, Santa Cruz, Santa Cruz, California 95064*

We have measured the uniaxial stress dependence of phonon absorption lines in KBr doped with $Li^+$ over the frequency range $75-225$ GHz. Several zero-stress lines are observed which exhibit a large ($\sim 40\%$) isotope shift when $^6Li$ replaces $^7Li$, clearly indicating a tunneling behavior. The general behavior of this system including the magnitude of the stress coupling is similar to other paraelectric-paraelastic centers found in the alkali halide. However, in detail, it is more complex than expected from the simple off-center tunneling models. Similar results were found earlier in an extensive paraelectric resonance study. These investigations indicate the need for further theoretical work.

## I. INTRODUCTION

We have studied the paraelastic behavior of KBr doped with $Li^+$ using phonon spectroscopy and observed a tunneling behavior similar to that found earlier in paraelectric resonance (PER) studies.[1] This is, therefore, the second major experiment in which the tunneling behavior of KBr:$Li^+$ is clearly exhibited. In addition, the shifts of the resonances both with uniaxial stress and with electric field are comparable in magnitude to those observed in other paraelectric-paraelastic systems.[2] The detailed behavior of this system, however, is quite unusual in many respects. First, the PER experiments[1] indicate that $Li^+$ has a strong tendency to clump or react with other impurities in the crystal and the lack of observable effects in early investigations can be understood if one assumes that only a small fraction of the lithium dopant exists as isolated ions. A second unusual feature of this system is that it has very large zero-field splittings. In the PER data, splittings of 140 and 160 GHz were observed for $^7Li$ and a yet larger splitting at 218 GHz has been found in the present study. In addition, the PER spectra has more structure than for any other monatomic off-center paraelectric system[2,3,4] and, therefore, provided a particularly strong test of the theoretical models. However, attempts to fit that data to the standard models met with limited success.

In this paper we present the phonon transmission spectra for single crystals of KBr:$^6Li^+$ and KBr:$^7Li^+$ over the frequency range $75-225$ GHz. Several absorption lines are clearly observed and their positions as a function of uniaxial stress were measured for three stress orientations over the range $0-1000$ bars. Attempts to explain these data in terms of the simple tunneling models[5] also were not very successful; consequently we include a brief discussion of some possible extensions of the tunneling models which might provide a better description of this unusual $Li^+$ system.

## II. SAMPLE PREPARATION AND EXPERIMENTAL TECHNIQUES

The KBr crystals were grown at the University of Utah from ultrapure starting material, with $10^{-3}$ to $10^{-2}$ mole fraction of LiBr added to the melt. In Table I we give details of the boules used in this work. The samples, typically $3 \times 4 \times 12$ mm$^3$ in size, were cut such that the major axis, along which the stress was applied, was parallel to a $\langle 100 \rangle$, $\langle 110 \rangle$, or $\langle 111 \rangle$ direction. Using x-ray diffraction we aligned the samples to within $1°$ of the desired orientation.

Phonons were transmitted through the sample in a direction perpendicular to the applied stress axis. For sample with $\vec{P} || \langle 100 \rangle$ and $\vec{P} || \langle 110 \rangle$ we chose a $\langle 100 \rangle$ propagation direction because for this orientation, the longitudinal phonon intensity is strongly enhanced by phonon focusing.[6] A $\langle 100 \rangle$ phonon path was not feasible for $\vec{P} || \langle 111 \rangle$; conse-

TABLE I. KBr Crystals.

| Boule | Li$^+$ melt concentration | Isotope | Comments |
|-------|---------------------------|---------|----------|
| 442[a] | $5 \times 10^{-3}$ | $^7$Li$^+$ | Used in PER experiments. |
| 1406[a] | $5 \times 10^{-3}$ | $^7$Li$^+$ | Atomic absorption measurement of Li$^+$ concentration—176 ppm top, 262 ppm bottom |
| 1475 | $10^{-2}$ | $^7$Li$^+$ | Most of $^7$Li$^+$ measurements. |
| 1498 | $5 \times 10^{-3}$ | $^6$Li$^+$ | All $^6$Li$^+$ measurements. |

[a]Samples destroyed.

quently we propagated the phonons along $\langle 1\bar{1}0 \rangle$, which resulted in a much weaker signal intensity.

Monochromatic phonons were generated and detected with superconducting tunnel junctions, using the technique developed by Kinder[7] A tin junction served as a generator with a frequency range up to 290 GHz and an aluminium junction as a detector with a sensitivity threshold near 80 GHz. A narrow band of phonon frequencies can be generated by modulating the generator voltage either with pulses or with an ac signal. With the pulse technique one can independently measure the phonon absorption of the various phonon modes. The ac method on the other hand usually gives a better signal-to-noise ratio and also provides a means of obtaining the first derivative of the absorption signal, but at the expense of no phonon mode differentiation. We generally used the latter method and found the absorption derivative signal particularly useful in resolving lines as they crossed or merged.

The crystal surfaces on which the tunnel junctions were to be evaporated had to be polished very carefully. For polishing we used a 1-$\mu$m Al$_2$O$_3$ powder on a "Mecaprex NV" polishing cloth, which we soaked with a mixture of methanol and a few percent of water. The cloth was allowed to dry almost completely before being used for polishing. Residual humidity was removed from the crystal surface by heating the sample to 150 °C for 20 min prior to evaporation.

To apply uniaxial stress on the relatively soft and fragile samples, we used the apparatus shown in Fig. 1. A force of up to 2500 N was produced by an air-driven piston at the top of the cryostat, by applying air pressures of up to 18 bars. The force was transferred to the sample via a stainless-steel pushrod. The net force reaching the sample

was measured by a Kistler quartz transducer which formed the support for the lower anvil. This force gauge was recalibrated for work at liquid-helium temperatures but the correction was less than 2%.

The ends of the samples were ground as flat and as parallel as possible using a (flat) brass jig. To compensate for small errors in making the ends parallel, the upper anvil consisted of a half spherical steel ball which could rotate inside a brass cone on the end of the push rod. (See Fig. 1.) Cardboard fastened to each of the anvils took up small irregularities of the surfaces.
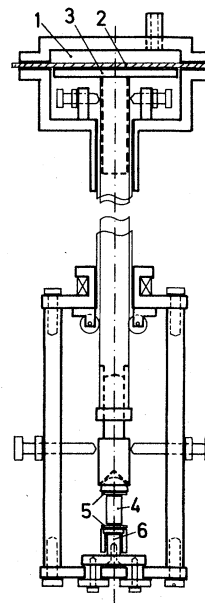


FIG. 1. Experimental apparatus for applying uniaxial pressure to the KBr crystals. 1. Compressed air chamber. 2. Rubber diagram. 3. Piston on top of push-rod. 4. Sample. 5. Upper (rotatable) and lower anvils. 6. Force gauge.

The homogeneity of the stress was checked by measuring the strain on opposite sides of a sample using identical strain gauges. After alignment of the upper and lower anvils to with 0.1 mm and centering the sample to within 0.2 mm, the stress (typically) turned out to be uniform to within 5%.

## III. THEORETICAL BACKGROUND

One type of paraelastic-paraelectric tunneling system is formed when a small impurity ion occupies an off-center position in the host crystal lattice. For cubic systems the simplest sets of *equivalent* off-center positions are directed along the 6 $\langle 100 \rangle$, the 8 $\langle 111 \rangle$, or the 12 $\langle 110 \rangle$ orientations. Each of these three systems is described using a multiwell potential model with minima in each of the equivalent off-center directions.

In the limit of infinite barriers between the wells the ground-state energy is 6-, 8-, or 12-fold degenerate for the above systems. If rotations of the off-center dipole from one orientation to another (i.e., movement of the impurity ion from one potential well to another) are assumed to occur via a tunneling mechanism this degeneracy is lifted in a manner consistent with the cubic symmetry of the host lattice. The resulting energy level splittings are referred to as zero-field or tunneling splittings and depend on the size of the tunneling parameters which parametrize tunneling through different rotation angles. Using the notation of Gomez et al.,[5] two parameters $\eta$ and $\mu$ are needed for a $\langle 100 \rangle$ system (90° and 180° tunneling), three parameters $\eta$, $\mu$, and $\nu$ for a $\langle 111 \rangle$ system (70°, 110°, and 180° tunneling), and four parameters, $\eta$, $\mu$, $\nu$, and $\sigma$ for a $\langle 100 \rangle$ system (60°, 90°, 120°, and 180° tunneling). The energy levels of the (zero-field) ground-state multiplet can be found in many earlier papers.[2,3,5]

If a uniaxial stress is also applied to a crystal, the degeneracy of these tunnel-split levels can be lifted further, and in the limit of large stress (stress energy >> zero-field splittings) the energy levels vary linearly with stress. The stress interaction is usually described using the stress dipole model of Nowick and Heller[8] and for the three simple cases considered above, only $E_g$ and $T_{2g}$ applied stress are expected to have a major effect. $A_{1g}$ stress, which is also present, often produces a relatively small shift in the energy levels, that is usually interpreted as a stress dependence of the tunneling parameters. We will neglect such effects in our analysis.

The coupling to $E_g$ and $T_{2g}$ external stress is parametrized using the stress "dipole moments" $\alpha_1(E_g)$ and $\alpha_2(T_{2g})$.[2] A $\langle 100 \rangle$ system couples only to $E_g$ stress, a $\langle 111 \rangle$ system only to $T_{2g}$ stress, while a $\langle 110 \rangle$ system couples to both types of stress.

For intermediate values of applied stress one must include both the tunneling (crystal field) Hamiltonian and the stress interaction to obtain the energy levels as a function of stress. This $12 \times 12$ matrix has usually been solved numerically in previous studies but simple analytic solutions can be obtained for $\vec{P} || \langle 100 \rangle$ and $\langle 111 \rangle$ using group theory. Some of the energy levels for $\vec{P} || \langle 110 \rangle$ also have simple analytic expressions. The energy levels for these cases are given in the Appendix.

## IV. DATA PRESENTATION

Measurements of the phonon absorption as a function of uniaxial stress were taken at $T = 0.95$ K over the frequency range 75–225 GHz. In Fig. 2 we show the transmission spectra for KBr:$^7$Li$^+$ at various pressures applied along a $\langle 111 \rangle$ orientation. The rapid increase in phonon transmission
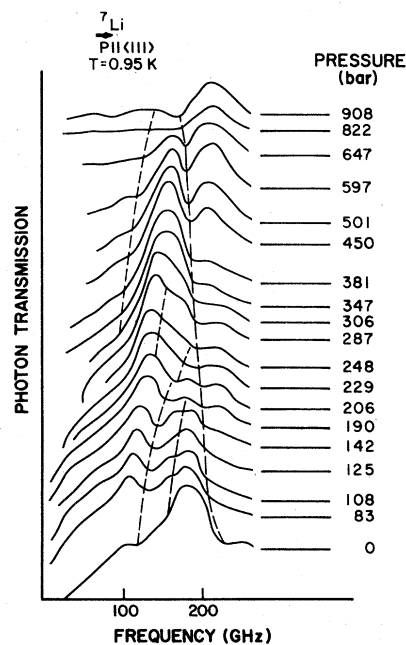


FIG. 2. Transmission spectra for KBr:$^7$Li$^+$ as a function of uniaxial pressure along a $\langle 111 \rangle$ orientation from 0 to 900 bars. Dotted lines connect a given line from trace to trace.
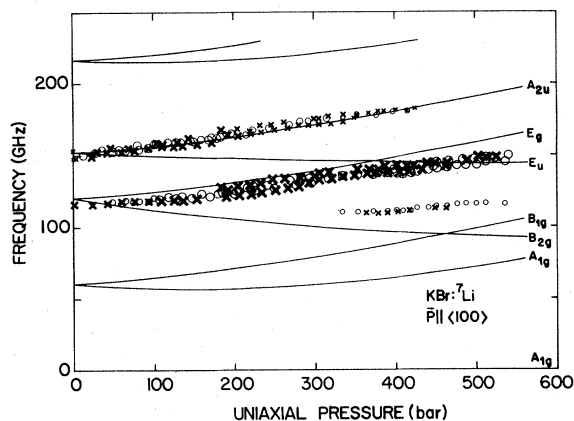
FIG. 3. Composite plot of the line positions for KBr:$^7$Li$^+$ as a function of uniaxial pressure $P$ for $P$ parallel to $\langle 100 \rangle$. The size of the data point roughly indicates the strength of the line, both here and in Figs. 4 and 5. The solid lines (here and in Figs. 4 and 5) are attempts to fit the data to a $\langle 110 \rangle$ model. See Sec. V.

signal that occurs near 100 GHz (Fig. 2) corresponds to the turn on of the detector diode. The overall decrease in signal intensity at high frequencies is a result of loss in the KBr sample and occurs in pure KBr as well as in $^7$Li$^+$ doped samples shown here.

On top of the overall transmission, several absorption dips are observed (Fig. 2) which are attributed to the $^7$Li$^+$ dopant. These lines shift when a uniaxial stress $P$ is applied and in Figs. 3−5 we present the composite plots of the line positions as a function of stress for $P$ parallel to $\langle 100 \rangle$, $\langle 111 \rangle$, and $\langle 110 \rangle$, respectively.
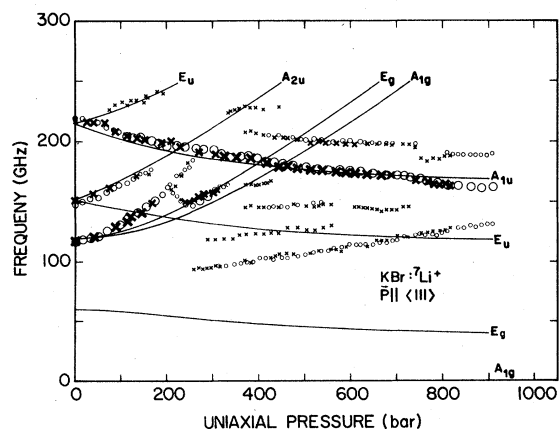
For samples doped with $^6$Li$^+$, the entire spec-



FIG. 4. Composite plot of the line positions KBr:$^7$Li$^+$ as a function of uniaxial pressure $P$ for $P$ parallel to $\langle 111 \rangle$.



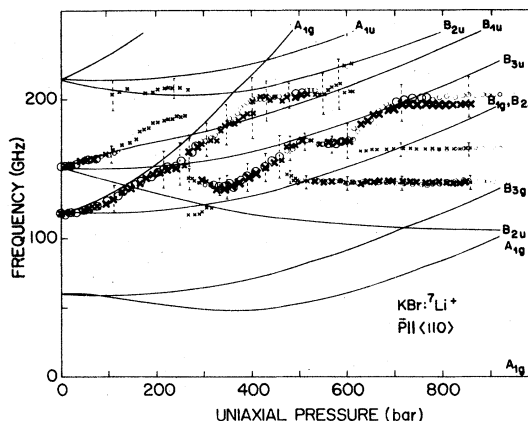FIG. 5. Composite plot of the line positions for KBr:$^7$Li$^+$ as a function of uniaxial pressure for $P$ parallel to $\langle 110 \rangle$.

trum changes (Fig. 6), with most of the lines moving to higher frequencies. For this isotope, data were only taken for $\vec{P}||\langle 100 \rangle$ (Fig. 7) and $\vec{P}||\langle 110 \rangle$ (Fig. 8).

The data for $\vec{P}||\langle 100 \rangle$ show little structure for both Li$^+$ isotopes (Figs. 3 and 7). In each case only a few lines are observed which shift slowly and linearly with applied uniaxial pressure at a rate of $0.06 \pm 0.01$ GHz/bar. Note that the shift is the same for both isotopes. However, the zero-filled splittings are large and the isotope shift of the dominant line is from 118−162 GHz—a 37% shift.

For $\vec{P}||\langle 110 \rangle$ several lines were observed, many of which show considerable structure. Some lines show a steplike behavior at higher frequencies (higher stress) suggesting the crossing of two or more resonance lines. For example, in the Li$^7$ data, steps occur at 160 GHz for $P \cong 500$ bars and at 195 GHz for $P$ approximately 700 bars. Ignoring the steplike structure, the general shift of the
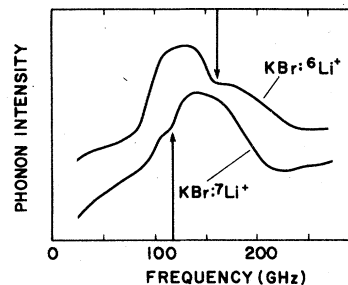


FIG. 6. Comparison of the transmission spectrum for $^6$Li$^+$ and $^7$Li$^+$ in KBr at zero stress. The main line for each isotope is indicated by an arrow.
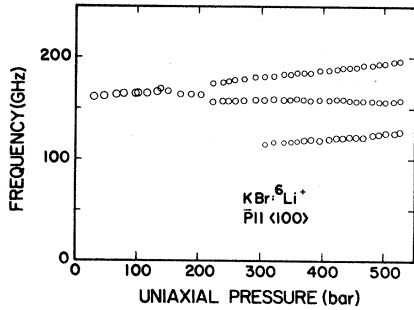
FIG. 7. Composite plot of the line positions for KBr:$^6$Li$^+$ with uniaxial pressure parallel to $\langle 100 \rangle$.

resonance lines with uniaxial pressure is in the range 0.16—0.22 GHz/bar. In addition, for the Li$^6$ data one weaker but well-defined line has a more rapid stress dependence of 0.33—0.37 GHz/bar. The zero-field splittings for this orientation agree with those observed for the $\vec{P} || \langle 100 \rangle$ data and again exhibit a large isotope shift.

Data for $\vec{P} || \langle 111 \rangle$ were only taken for the $^7$Li isotope (Fig. 4) and are surprising in several respects. Firstly, the *relative* absorption for phonons propagating along a $\langle 1\bar{1}0 \rangle$ orientation is much stronger than for $\langle 100 \rangle$ propagation. This was an important factor in obtaining good $\vec{P} || \langle 111 \rangle$ data since the overall phonon intensity for transmission along $\langle 1\bar{1}0 \rangle$ is much smaller than along $\langle 100 \rangle$ as a result of defocusing. Secondly, several lines are observed with quite different stress dependencies, The main line at low stress has a zero-field splitting of 118 GHz, and increases non-linearly with stress up to about 200 bars. Near 210 bars this line essentially disappears while at slightly higher pressures several new lines emerge which are relatively weak. Another fairly strong line starts at 150 GHz and moves more or less linearly with stress until it disappears around 180—190
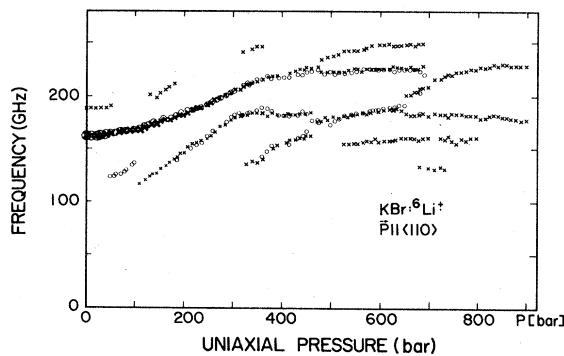


FIG. 8. Composite plot of the line positions for KBr:$^6$Li$^+$ with uniaxial pressures parallel to $\langle 110 \rangle$.

bars. A weaker line with a splitting of 218 GHz has a similar behavior. A more surprising feature of the data (Fig. 4) is the presence of a very strong backward line (a line that moves to lower frequency with increasing $P$) also with a zero-field splitting of 218 GHz. This line is strong over the entire range of pressure up to 900 bars which indicates it must originate from one of the lowest energy levels of this system. Although many of the lines vary nonlinearly with stress we can roughly characterize the stress dependence of the two main lines [with zero-field splitting (zfs) of 118 and 150 GHz] in the low stress regime as 0.25 GHz/bar. The measured zero-field splittings and the shifts of the resonance lines with stress are tabulated in Table II.

## V. DATA ANALYSIS

The fact that the observed line positions and relative intensities are always consistent for each boule doped with a particular Li$^+$ isotope, suggests that the observed signal arises from a single impurity center rather than a distribution of different centers. In addition, several of the samples came from boules used in the PER work. In that investigation, many different boules were used, which gave the same PER spectra. This strengthens our assertion that a single center is involved and in the following analysis this point will be assumed.

The isotope shift of the zero-field splittings is a large and striking effect. When $^6$Li$^+$ replaces $^7$Li$^+$ as the dopant, the entire spectrum shifts indicating that the observed center involves the Li$^+$ ion. This is further evidence for a single center. In addition, the large 37% isotope shift of the main zero-field splitting is close to the shift observed in the PER work although different transitions are observed, and is also very close to the isotope shift observed in KCl:Li$^+$. It is much *larger than the change in the Li$^+$ mass (17%)*, indicating that the Li$^+$ ion is *tunneling* between potential wells rather than *oscillating* in a simple potential well.

Our first step was to compare the data with the general predictions of the simple tunneling models. We immediately rejected the $\langle 100 \rangle$ and $\langle 111 \rangle$ models since they (i) give only two or three independent zero-field splittings, (ii) should have no stress dependence for some orientations of uniaxial pressure, and (iii) have only one value of the slope (i.e., the frequency shift per bar in Figs. 3—5) for each of the other orientations.[2]

Even the $\langle 110 \rangle$ model does not have enough en-

TABLE II. Zero-field splittings and line shifts with stress for main lines for $^7Li^+$.

| Zero-field splitting | Shift of line with stress | | | Comments |
|---|---|---|---|---|
| | $\vec{P}||\langle 100 \rangle$ | $\vec{P}||\langle 111 \rangle$ | $\vec{P}||\langle 110 \rangle$ | |
| 118 GHz | $\simeq 0.06$ GHz/bar | $\simeq 0.25$ GHz/bar | $\simeq 0.23$ GHz/bar | Dominant line |
| 150 GHz | 0.075 GHz/bar | $\simeq 0.20$ GHz/bar | $\simeq 0.020$ GHz/bar | Decrease in intensity for all stress orientations. |
| 218 GHz | | negative shift, $\simeq - 0.16$ GHz/bar | | Strong line in $\langle 111 \rangle$ orientation |
| | | $\simeq 0.14$ GHz | $(\sim 0$ GHz/bar$)$ | Weak line |
| $< 100$ GHz | | 0.06 GHz/bar | $\simeq 0.17$ GHz/bar? | zfs not clear |

ergy levels to explain all the observed zero-field splittings (in PER and phonon measurements). However, most of the general features of the data are consistent with a $\langle 110 \rangle$ model and we have, therefore, attempted to fit the main $^7Li^+$ lines to this simple model.

To carry out this analysis we need estimates of the two stress coupling constants, $\alpha_1$ and $\alpha_2$, and some criteria by which we can assign the observed transitions to the possible theoretical ones. As a first approximation, we used the slope observed in the $\langle 100 \rangle$ data for $\alpha_1$ and the main slope from the $\langle 111 \rangle$ data for $\alpha_2$. Since we are not really in the high field limit, we expected both these values to be $20-30\%$ low, and varied these parameters to obtain a better fit to the observed line shifts with stress.

In our first attempts, instead of matching possible theoretical and experimental transitions, we used the sets of tunneling parameters which give some of the better fits to the PER data. Unfortunately, all gave very poor agreement. The major problem in all cases is that these sets of parameters do not predict the zero-field splittings of all the *main* phonon lines. This was not totally unexpected since the allowed transitions in PER are different from the phonon transitions and the total number of independent zfs observed in both types of measurements exceeds the number expected for a $\langle 110 \rangle$ system.

To see how well the phonon data alone could be fit to a $\langle 110 \rangle$ model we assumed that all observed transitions originate from an $A_{1g}$ ground state (all observed zero-field splittings are large, $> 3K$, and data were taken at 0.95 K). We used the observed phonon zero-field splittings of $^7Li^+$ at 218, 150,

and 118 GHz plus a fourth splitting near 60 GHz. Although we could not see the latter, the PER data have many lines with zero-field splittings between 50 and 65 GHz and some lines in the phonon data indicate a splitting below 100 GHz. We then examined the data for possible constraints on the ordering of the zero-field energy levels. As an example, consider the strong backward line in the $\langle 111 \rangle$ data with a zfs of 218 GHz. The analytic solutions for the energy levels (Appendix) indicate that this transition can be at most one of three, $A_{1g}$ to $A_{1u}$, $E_u$ or $E_g$, with the $A_{1g}-A_{1u}$ giving the most pronounced backward line. In addition, a second weak line in the $\langle 111 \rangle$ data also has a zfs of 218 which means that this energy level must split under $\langle 111 \rangle$ uniaxial stress. Thus, this zero-field transition must be to either the $T_{1u}$ or $T_{2u}$ state.

Several different assignments were tried and *partial* fits were achieved, with the best fit obtained using the parameters $\eta,\mu,\nu,\sigma = -13$, $-20$, 3, $-52$ GHz $\alpha_1 = 0.13$ GHz/bar and $\alpha_2 = 0.31$ GHz/bar. This fit is shown by the solid lines in Figs. 3—5 for $^7Li^+$. Although quite a few experimental lines agree well with the theory, including the backward $\langle 111 \rangle$ line, some lines are not predicted at all, while others are not allowed for phonons of either $E_g$ or $T_{2g}$ symmetry. One must assume some $T_{1u}$ or $T_{2u}$ component in the phonon pulse or some other interaction which mixes states to explain the intensity of such transitions.

This partial fit is quite comparable to that obtained for the PER data. The fact that the *same* parameters can fit several lines in *each* orientation of applied uniaxial stress indicates that this tunneling system has the expected overall cubic symmetry of the host lattice. However, the large

number of zfs observed in the phonon and PER experiments plus the extra lines that cannot be fit using a $\langle 110 \rangle$ tunneling model suggest a *more complicated system* which exhibits many of the properties of a $\langle 110 \rangle$ system. A complex $Li^+$ center in which the $Li^+$ is off center *only* as a result of some nearest neighbor atom $X$ is not a viable possibility since such complexes should have a restricted number of off-center positions and consequently a simpler structure—even when all static orientations of the $Li^+X$ complex are considered.

Before leaving the $\langle 110 \rangle$ model we should mention that we included the overlap parameters in some of our calculations of the energy levels. This leads to modified slopes in the high stress limit, and in a few cases to some additional slopes, but does not give any additional zfs which are needed to explain both the PER and phonon results.

Since no other tunneling models have been developed in detail as yet, we consider some particular features of the data and some possible explanations for them. These ideas are of course speculative at this point.

(1) The many lines which are internally consistent with each other, together with the extra slopes in the $\langle 111 \rangle$ data and the steplike nature of some of the high-frequency data, indicative of resonance line crossings, suggests a more complicated model that can also appear to be a $\langle 110 \rangle$ model under some choices of parameters. One type of model which will do this and still be consistent with cubic symmetry is a 24-fold potential well system. Although such models have been disregarded in the past because such a highly convoluted potential surface seems unreasonable, the complexity of the present data is in keeping with a more complicated model.

At least three such systems exist, one with two potential wells on each edge of a cube, one with four potential wells on each face of a cube, situated near the middle of the cube edges, and one with four potential wells on a face, situated near the corners (See Fig. 9). The first two could appear very similar to a $\langle 110 \rangle$ model if the two wells on an edge in the first case or near an edge in the second, are very close together. This could lead to pseudo-$\langle 110 \rangle$-like behavior, and in the case where the tunneling between these two closely adjacent wells is very large, might lead to behavior similar to that of a two-multiplet system.

(2) The strong backward line and the apparent crossings of energy levels might also be the result of a two multiplet structure with a multiplet split-
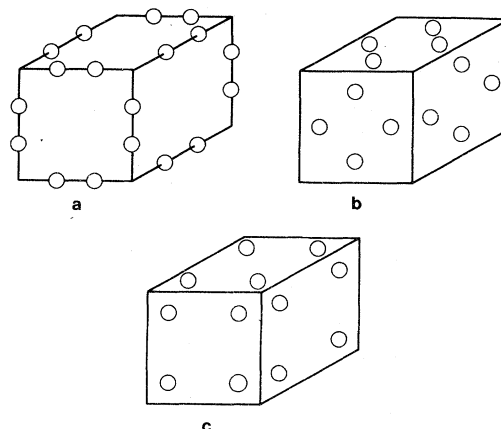


FIG. 9. Three possible 24-well potentials. The spheres represent the positions of off-center potential wells about a lattice site at the center of the cube. The spheres on the back faces of the cube are not shown.

ting of 150—300 GHz. Such an energy level structure has been observed[9] in KI:OH$^-$ and low-lying far-infrared modes have been found in several systems. Luty[10] expects that such multiplet structures will be found for many paraelectric systems. For diatomic ions with both an intrinsic dipole moment and the possibility of an off-center dipole, it is easy to see how two closely spaced multiplets might form (one for each type of dipole). For the simple ions such as $Li^+$ such an explanation does not work, and other means of achieving a two multiplet structure must be found. If one considers the second energy level in each of the separate off-center wells one finds that for free isolated $Li^+$ ions, these levels are more than 500 GHz above the ground state. A very strong effective-mass renormalization (which takes into account the lattice distortions about the site) would be necessary to bring this splitting into a range consistent with the data. Because of the strong isotope shift, this does not appear likely for KBr:$Li^+$.

Another possibility for a two multiplet type of energy level structure is to have a thirteenth potential well on the symmetry site as proposed by Holland and Luty[11] for RbCl:$Ag^+$. Assuming the ground state of this well to be $\epsilon_0$ above or below the ground states of the off-center wells one obtains an energy-level scheme with a single additional level above or below the tunneling multiplet. Although we have not considered this possibility in detail, a preliminary investigation suggests that it is not very promising. The matrix elements connecting this on-center well to each of the off-center

wells must be the same by symmetry. Consequently, if this extra level does not shift with external fields or stress, backward-type lines should be observed in both the PER and phonon experiments for most electric-field—uniaxial-stress orientations, in contrast to the observations.

## VI. SUMMARY

The phonon absorption data presented in this paper are in general agreement with the results obtained using paraelectric resonance. KBr doped with $Li^+$ forms a paraelectric-paraelastic center in which $Li^+$ is the tunneling entity. This system does have many general features of the simple $\langle 110 \rangle$ model and in terms of a very crude analysis the stress coupling parameters can be obtained. However, as in the PER data, several lines are not explained and a detailed fit of theory and experiment cannot be obtained with the simple models. Because of the large number of zero-field splittings and the number of lines that cannot be explained within a simple $\langle 110 \rangle$ model we believe a more complicated model, such as a 24-dipole system or one with additional excited states, will be necessary before one can understand the behavior of this unusual tunneling system.

## ACKNOWLEDGMENTS

## APPENDIX: ANALYTIC EXPRESSIONS FOR THE ENERGY LEVELS OF A $\langle 110 \rangle$ SYSTEM IN THE PRESENCE OF UNI AXIAL STRESS

In the following equations, $\eta$, $\mu$, $\nu$, and $\sigma$ are the tunneling elements as defined by Gomez et al.,[5] $\alpha_1$ and $\alpha_2$ are the stress coupling constants,[8,2] and $P$ is the uniaxial stress. The symmetry of each level is also indicated.

(a) $\vec{P} || \langle 100 \rangle$:

$$E_1(A_{1g}) = -\tfrac{1}{6}\alpha_1 P + \eta + 2\mu + \nu + \sigma$$
$$+ [(\tfrac{1}{2}\alpha_1 P + \eta + \nu)^2 + 8(\eta + \nu)^2]^{1/2},$$

$$E_2(A_{1g}) = -\tfrac{1}{6}\alpha_1 P + \eta + 2\mu + \nu + \sigma$$
$$-[(\tfrac{1}{2}\alpha_1 P + \eta + \nu)^2 + 8(\eta + \nu)^2]^{1/2},$$

$$E(A_{2u}) = \tfrac{1}{3}\alpha_1 P + 2\eta - 2\nu - \sigma,$$

$$E(B_{2u}) = \tfrac{1}{3}\alpha_1 P - 2\eta + 2\nu - \sigma,$$

$$E(B_{1g}) = \tfrac{1}{3}\alpha_1 P - 2\eta + 2\mu - 2\nu + \sigma,$$

$$E(B_{2g}) = -\tfrac{2}{3}\alpha_1 P - 2\mu + \sigma,$$

$$E(E_g) = \tfrac{1}{3}\alpha_1 P - 2\mu + \sigma,$$

$$E_{1,2}(E_u) = -\tfrac{1}{6}\alpha_1 P - \sigma + [(\tfrac{1}{2}\alpha_1 P)^2 + 4(\eta - \nu)^2]^{1/2},$$

$$E_{1,2}(E_u) = -\tfrac{1}{6}\alpha_1 P - \sigma - [(\tfrac{1}{2}\alpha_1 P)^2 + 4(\eta - \nu)^2]^{1/2}.$$

(b) $\vec{P} || \langle 111 \rangle$:

$$E_{1,2}(A_{1g}) = 2(\eta + \nu) + \sigma$$
$$\pm [\tfrac{1}{4}(\alpha_2 P)^2 + 4(\eta + \mu + \nu)^2]^{1/2},$$

$$E(A_{1u}) = -\tfrac{1}{2}\alpha_2 P - 2\eta + 2\nu - \sigma,$$

$$E(A_{2u}) = \tfrac{1}{2}\alpha_2 P + 2\eta - 2\nu - \sigma,$$

$$E_{1,2}(E_u) = -\sigma + [(\tfrac{1}{2}\alpha_2 P + \eta - \nu)^2 + 3(\eta - \nu)^2]^{1/2},$$

$$E_{3,4}(E_u) = -\sigma - [(\tfrac{1}{2}\alpha_2 P + \eta - \nu)^2 + 3(\eta - \nu)^2]^{1/2},$$

$$E_{1,2}(E_g) = \sigma - \eta - \nu + [(\tfrac{1}{2}\alpha_2 P)^2 + (2\mu - \eta - \nu)^2]^{1/2},$$

$$E_{3,4}(E_g) = \sigma - \eta - \nu - [(\tfrac{1}{2}\alpha_2 P)^2 + (2\mu - \eta - \nu)^2]^{1/2}.$$

(c) $\vec{P} || \langle 110 \rangle$. In this case a simple set of analytical solutions is not possible, although one can in principle obtain solutions to the remaining $3 \times 3$ determinant. The following nine analytical solutions are given, together with the $3 \times 3$ matrix that must be solved to obtain the three $A_{1g}$ states:

$$E(B_{1g}) = -\tfrac{1}{6}\alpha_1 P - 2\mu + \sigma,$$

$$E(B_{2g}) = -\tfrac{1}{6}\alpha_1 P - 2\mu + \sigma,$$

$$E(B_{3g}) = -\tfrac{1}{6}\alpha_1 P - 2\eta + 2\mu - 2\nu + \sigma,$$

$$E(A_{1u}) = -\tfrac{1}{6}\alpha_1 P - 2\eta + 2\nu - \sigma,$$

$$E(B_{3u}) = -\tfrac{1}{6}\alpha_1 P + 2\eta - 2\nu - \sigma,$$

$$E_{1,2}(B_{1u}) = \tfrac{1}{2}(\tfrac{1}{6}\alpha_1 + \tfrac{3}{4}\alpha_2)P$$
$$\pm [(\tfrac{1}{4}\alpha_1 P + \tfrac{3}{8}\alpha_2 P)^2 + 4(\eta - \nu)^2]^{1/2} - \sigma,$$

$$E_{1,2}(B_{2u}) = \tfrac{1}{2}(\tfrac{1}{6}\alpha_1 - \tfrac{3}{4}\alpha_2)P$$
$$\pm [(\tfrac{1}{4}\alpha_1 P - \tfrac{3}{8}\alpha_2 P)^2 + 4(\eta - \nu)^2]^{1/2} - \sigma,$$

and the matrix for $A_{1g}$ states is

$$\begin{bmatrix} 4\eta+2\mu+4\nu+\sigma & -\alpha_1 P/3\sqrt{2} & 3\alpha_2 P/2\sqrt{12} \\ -2\alpha_1 P/6\sqrt{2} & -2\eta+2\mu-2\nu+\sigma+\frac{1}{6}\alpha_1 P & -3\alpha_2 P/\sqrt{24} \\ 3\alpha_2 P/4\sqrt{3} & -3\alpha_2 P/\sqrt{24} & -2\mu+\sigma+2\alpha_1 P/6 \end{bmatrix} .$$

[1]F. Bridges and R. S. Russell, Solid State Commun. 21, 1011 (1977); R. S. Russell, Ph.D. thesis, University of California, Santa Cruz, 1978 (unpublished).

[2]F. Bridges, Crit. Rev. Solid State Sci. 5, 1 (1975).

[3]R. A. Herendeen and R. H. Silsbee, Phys. Rev. 188, 645 (1969).

[4]D. Blumenstock, R. Osswald, and H. C. Wolf, Z. Phys. 231, 333 (1970); Phys. Status Solidi B 46, 217 (1971).

[5]M. Gomez, S. P. Bowen, and J. A. Krumhansl, Phys. Rev. 153, 1009 (1967).

[6]H. J. Maris, J. Acoust. Soc. Am. 50, 812 (1971).

[7]H. Kinder, Phys. Rev. Lett. 28, 1564 (1972); Z. Phys. 262, 295 (1973).

[8]A. S. Nowick and W. R. Heller, Adv. Phys. 12, 251 (1963).

[9]W. Kelly and F. Bridges, Phys. Rev. B 18, 4606 (1978).

[10]F. Luty (private communication).

[11]U. Holland and F. Luty, Phys. Rev. B 19, 4298 (1979).